GASTROENTEROLOGY

Contribution of upregulated aminoacyl-tRNA biosynthesis to metabolic dysregulation in gastric cancer

Xiaoling Gao,*,[†1] Rui Guo,*,[†1] Yonghong Li,*,[†1] Guolan Kang,[‡] Yu Wu,* Jia Cheng,[‡] Jing Jia,* Wanxia Wang,* Zhenhao Li,* Anqi Wang,* Hui Xu,[†] Yanjuan Jia,[†] Yuanting Li,[†] Xiaoming Qi,[†] Zhenhong Wei[†] and Chaojun Wei*,[†]

*NHC Key Laboratory of Diagnosis and Therapy of Gastrointestinal Tumor, [†]The Institute of Clinical Research and Translational Medicine, [‡]Department of Endoscopic Diagnosis and Treatment Center, Gansu Provincial Hospital, Lanzhou, China

Correspondence

Dr Chaojun Wei and Dr Xiaoling Gao, NHC Key Laboratory of Diagnosis and Therapy of Gastrointestinal Tumor, Gansu Provincial Hospital, 204 Donggang West Road, Chengguan District, Lanzhou 730000, China. Email: weichaojun-gsph@hotmail.com; gaoxl008@hotmail.com

Abstract

Background and Aim: Metabolic reprogramming is characterized by dysregulated levels of metabolites and metabolic enzymes. Integrated metabolomic and transcriptomic data analysis can help to elucidate changes in the levels of metabolites and metabolic enzymes, screen the core metabolic pathways, and develop novel therapeutic strategies for cancer.
Methods: Here, the metabolome of gastric cancer tissues was determined using liquid chromatography–mass spectrometry. The transcriptome data from The Cancer Genome Atlas dataset were integrated with the liquid chromatography–mass spectrometry data to identify the common dysregulated gastric cancer-specific metabolic pathways. Additionally, the protein expression and clinical significance of key metabolic enzymes were examined using a gastric cancer tissue array.
Results: Metabolomic analysis of 16 gastric cancer tissues revealed that among the 15 dysregulated metabolomic pathways, the aminoacyl-tRNA biosynthesis pathway in the gastric tissues was markedly upregulated relative to that in the adjacent noncancerous tissues, which was consistent with the results of transcriptome analysis. Bioinformatic analysis revealed that among the key regulators in the aminoacyl-tRNA biosynthesis pathway, the expression levels of threonyl-tRNA synthetase (TARS) and phenylalanyl-tRNA synthetase (FARSB) were correlated with tumor grade and poor survival, respectively. Additionally, gastric tissue array data analysis indicated that TARS and FARSB were upregulated in gastric cancer tissues and were correlated with poor prognosis and tumor metastasis.
Conclusions: This study demonstrated that the aminoacyl-tRNA biosynthesis pathway is upregulated in gastric cancer and both TARS and FARSB play key roles in the progression of gastric cancer. Additionally, a novel therapeutic strategy for gastric cancer was proposed that involves targeting the aminoacyl-tRNA biosynthesis pathway.

Introduction

Metabolites are the end products of the complex interactions between genetic and environmental factors. To meet the increased energetic and biosynthetic demands of proliferation, the cancer cells undergo metabolism reprogramming, which promotes the initiation and progression of human cancer, especially those of gastric cancer (GC).[1] Previous studies have reported that the metabolism of amino acids, lipids, glucose, and nucleotides is dysregulated in GC.[2–4] Hence, targeting metabolic pathways to elucidate the pathogenesis of GC and develop novel therapeutic strategies

for GC has piqued the interest of the scientific community. However, the role of metabolic pathways in the development of GC and the underlying mechanisms has not been elucidated.

Metabolomic reprogramming is classified into the following distinct phases: transcriptional activation of metabolic enzymes and accumulation of metabolites.[5,6] Multiple genes are involved in metabolic pathways that catalyze the production of upstream factors.[7,8] However, recent studies have focused on metabolite changes in GC rather than the effect of transcripts on GC metabolism. Therefore, there is a need to integrate metabolomic and transcriptomic analyses to identify the key metabolomic pathways in GC; this will enable the development of strategies to target the key metabolic pathways and consequently aid in the elucidation of the pathogenesis of GC and the development of novel therapeutic strategies.

In addition to facilitating comprehensive metabolite identification and quantification, high-throughput multi-omic data integration provides useful insights into cancer development based on the complete spectrum of endogenous metabolites.[9] High-throughput transcriptional and metabolic techniques capture metabolic signatures, such as metabolites, catalytic genes, and regulators involved in the biosynthetic pathways. Additionally, the integrated analysis of the metabolome and transcriptome data along with bioinformatic analysis will enable the identification of activated metabolic pathways and the metabolic pathways that are potential therapeutic targets.

This study sought to examine the specific metabolomic profile of GC, integrate the metabolomic data with the transcriptomic data, and determine the changes in gene expression. Pathway analysis was performed using pooled hub genes and significant metabolites. The metabolic and transcriptomic changes associated with GC were elucidated. The aminoacyl-tRNA biosynthesis pathway was found to be enriched and hyperactive in GC tissues. Additionally, a regulatory network was constructed to identify biosynthesis-related genes and regulators. The expression levels of the aminoacyl-tRNA synthesis enzymes, threonyl-tRNA synthetase (TARS) and phenylalanyl-tRNA synthetase (FARSB), were correlated with the malignancy and progression of GC. Furthermore, the functions of TARS and FARSB were analyzed, and their correlation with the malignancy and progression of GC was determined. This study revealed the catalytic characteristics of GC metabolism and provided novel insights into cancer etiology, which will facilitate the identification of promising therapeutic targets for GC.

Materials and methods

Study cohort. In this study, 16 patients with pathologically confirmed primary GC who had undergone surgical resection at the Gansu Provincial Hospital between 2018 and 2019 were included. The study subjects did not undergo drug therapy before the surgery. Cancer tissues and adjacent noncancerous tissues were subjected to metabolomic analysis. The study protocol was approved by the Ethics Committee of Gansu Provincial Hospital (2020-019). Written informed consent was obtained from all patients before sample collection.

The Cancer Genome Atlas Stomach Adenocarcinoma gene expression dataset was obtained from TCGA database (https://tcga-data.nci.nih.gov/tcga/). The dataset consisted of 32 adjacent noncancerous tissues and 375 GC tissues. Clinical data, such as sex, age, histological type, survival, and clinical outcomes, were also downloaded from TCGA database (Table S1).

Gastric tissue microarray (TMA, HStmA180Su15) was obtained from Outdo Biotech Co., Ltd. (Shanghai, China). The TMA consists of primary tumors, which were resected between 2006 and 2015, of 98 patients. Clinicopathological characteristics, including survival time, pathological grade, pathological stage, and immunostaining analysis of p53/ki67/CD133/VEGFR/E-cadherin of patients with GC, were collected. The tissues in the TMA were collected after ethical approval (YB M-05-02). The detailed characteristics of the TMA samples are presented in Table S2.

Liquid chromatography–tandem mass spectrometry analysis

Sample processing. For liquid chromatography–mass spectrometry analysis, 60-mg tissue sample was homogenized in 200-µL water and precooled 800-µL methanol/acetonitrile (1:1; v/v). The mixture was sonicated twice for 30 min and incubated at -20 °C for 1 h to precipitate the proteins. The samples were centrifuged at 12 000 *g* and 4 °C for 15 min, and the supernatant was subjected to freeze-drying and stored at -80 °C.

Liquid chromatography–tandem mass spectrometry analysis. The samples were resolved using high-performance liquid chromatography with an Agilent 1290 Infinity (Agilent Technologies, Wilmington, DE, USA) equipped with an Acquity UPLC BEH amide column (Waters, 1.7 µm, 2.1 × 100 mm) at 25 °C. The gradient mobile phase consisted of solvent A (ammonium hydroxide, acetic acid, and water) and solvent B (acetonitrile), and the flow rate of the mobile phase was 0.3 mL/min. The gradient elution conditions were as follows: 0–0.5 min, 95% B; 0.57 min, 95–65% B; 7–8 min, 65–40% B; 8–9 min, 40% B; 9–9.1 min, 40–95% B; and 9.1–12 min, 95% B. Quality control samples, which were pooled with equal aliquots of tissue samples, were analyzed throughout the experiment to monitor and evaluate the stability of the instrument and the reliability of the experimental data.

The samples were analyzed using an Agilent 6500 mass spectrometer (Agilent Technologies) equipped with an electrospray ionization (ESI) source in positive and negative ion modes. The ESI source conditions were as follows: gas temperature, 250 °C; drying gas flow rate, 16 L/min; nebulizer pressure, 20 psig; sheath gas temperature, 400 °C; sheath gas flow rate, 12 L/min; capillary voltage, 3000 V; nozzle voltage, 0 V; fragmentation voltage, 175 V; mass range, 50–1200; acquisition rate, 4 Hz; and cycle time, 250 ms.

Metabolites were identified using a Triple TOF 6600 mass spectrometer (AB Sciex, Redwood City, CA, USA). The ESI source conditions were as follows: ion source gas1 (Gas1), 40; ion source gas2 (Gas2), 80; curtain gas (CUR), 30; source temperature: 650 °C; and ion spray voltage floating, ±5000 V. MS/MS spectra were collected using information-dependent acquisition in a high-sensitivity mode. The structures of the metabolites were identified using the MetDDA and LipDDA methods (Shanghai Applied Protein Technology).

Data analysis. The raw data from liquid chromatography–tandem mass spectrometry (LC–MS/MS) were converted to .mzXML format files using the MS converter tool.[10] The peaks were identified using the XCMS program. The retention time was corrected, and the peak area was extracted. Data normalization and analysis were performed as previously described.[11] The not available values (NAs) were set when the peak intensities were recorded at 0 s. If NAs in the detected peaks of metabolite appear in more than two-thirds samples, the peaks were not included; otherwise, value imputation was performed using the *k*-nearest neighbor algorithm. Least squares support vector regression was used to normalize the peak intensity data. After normalization and integration of the peak intensity data, matrix data were generated, including sample names, retention time–*m/z* pairs, and normalized peak area percentages.

Gene set enrichment analysis. The significant differentially expressed metabolic pathways between adjacent noncancerous tissues and GC tissues were analyzed using gene set enrichment analysis (GSEA). GSEA provided a statistical method with a priori defined set of genes that can distinguish if the members of genes are randomly distributed between the two conditions (i.e. adjacent noncancerous tissues and GC tissues in this study).

The pre-ranked GSEA tool (GSEAPreRanked; http://www.broadinstitute.org/gsea/, version 4.0.2) was used to identify pathways that were differentially expressed in GC tissues. The raw transcriptomic profiles were inputted into the GSEA package. The pre-ranked GSEA tool utilizes the C2 curated gene sets (Kyoto Encyclopedia of Genes and Genomes [KEGG] gene sets). The permutation type was set to gene_set with 1000 permutations. The enrichment score (ES), which indicates the degree to which a set of genes is ranked, was calculated. The significance level of ES represents the complex correlation structure of the gene expression data.

Integration of metabolomic and transcriptomic analysis in gastric cancer. To identify the significant pathways in GC tissues and construct Venn diagrams, GC-related metabolomic pathways and transcriptomic pathways (from GSEA results) were inputted into the online tool, VENNY 2.1.0 (http://bioinfogp.cnb.csic.es/tools/venny/index.html).

Immunohistochemistry microarray analysis. The TMA slides were deparaffinized with xylene, dehydrated with graded alcohol washes, and incubated with antigenic retrieval buffer. The sections were incubated overnight at 4 °C with the anti-TARS (1:3000; Abcam, Cambridge, UK) and anti-FARSB (1:500; Abcam) antibodies. The sections were then washed and incubated with the secondary antibody for 30 min at 37 °C. Immunoreactive signals were visualized using diaminobenzidine. The sections were counterstained with hematoxylin for 1 min at 37 °C and mounted in neutral gum. The stained fields were imaged using a bright-field microscope and were evaluated by three experienced pathologists blinded to the clinical data. Immunohistochemical (IHC) score, which ranged from 0 to 3, was obtained by multiplying the staining intensity and the stained cell percentage scores. The expression levels of TARS and FARSB were

considered to be low if the final staining scores were in the range of 0–0.8 and 0–1.3, respectively. Meanwhile, the final staining scores in the range of 0.85–3 and 1.35–3 represented high expression levels of TARS and FARSB, respectively.

Statistical analysis. Multivariate processing of the MS data was performed using orthogonal partial least squares discriminant analysis (OPLS-DA) to generate models for the classification of GC and control groups. The OPLS-DA model was implemented in the SIMCA-P14.1 software using permutation tests with 200 random permutations. The variable importance in the projection from the OPLS-DA model was considered as a criterion for differential metabolite selection. MetaboAnalyst 3.0 was used for KEGG pathway enrichment analysis (https://www.metaboanalyst.ca/),[12] while Mev software was used for hierarchical clustering analysis.

The Wilcoxon test was used to examine the association between gene expression and clinicopathological parameters. The log-rank test was performed to compare the survival curves of the GC and control groups. Pearson's correlation coefficient was used to estimate the association between variables. The differences were considered significant at $P < 0.05$. The P values were adjusted using the Benjamini–Hochberg method. All statistical analyses were performed using R version 3.5.1.

Results

Dysregulated metabolic pathways in gastric cancer. To identify the specific metabolite features in GC, 16 paired cancer tissues and adjacent noncancerous tissues were subjected to LC–MS/MS analysis. The clinical characteristics of the patients are listed in Table S3. The total ion current chromatogram of the GC and adjacent noncancerous tissues is illustrated in Figure S1. Numerous signals detected within the total ion current chromatogram were identified as metabolites. OPLS-DA provides insights into the separation of metabolites between different groups. In both ESI+ and ESI− modes, the metabolites of the GC tissue exhibited distinct clustering from those of the adjacent noncancerous tissue (Fig. 1a). In total, 71 differentially expressed metabolites were screened (38 and 33 metabolites in ESI+ and ESI− modes, respectively) based on the following criteria: variable importance in the projection > 1 and $P < 0.05$ (Tables 1, 2). The differentially expressed metabolites mainly consisted of amino acids, carbohydrates, lipids, and nucleosides. Compared with those in the adjacent noncancerous tissues, the levels of amino acids were higher, whereas those of carbohydrates were lower in the GC tissues. Vertical cluster analysis revealed the differential metabolic profile between GC and adjacent noncancerous tissues. The distribution patterns of 71 potential metabolites were displayed using a heatmap (Fig. 1b).

To explore the mechanism underlying GC metabolism and comprehensively characterize the differential metabolites, 71 differentially expressed metabolites were combined for subsequent analysis. KEGG pathway enrichment analysis and topology analysis were performed to preliminarily assess the biological functions of 71 differential metabolites in GC (Fig. 1c). The analysis revealed the clustering of 15 metabolic pathways (Table S4). Aminoacyl-tRNA biosynthesis; glycine, serine, and threonine

a

b

c
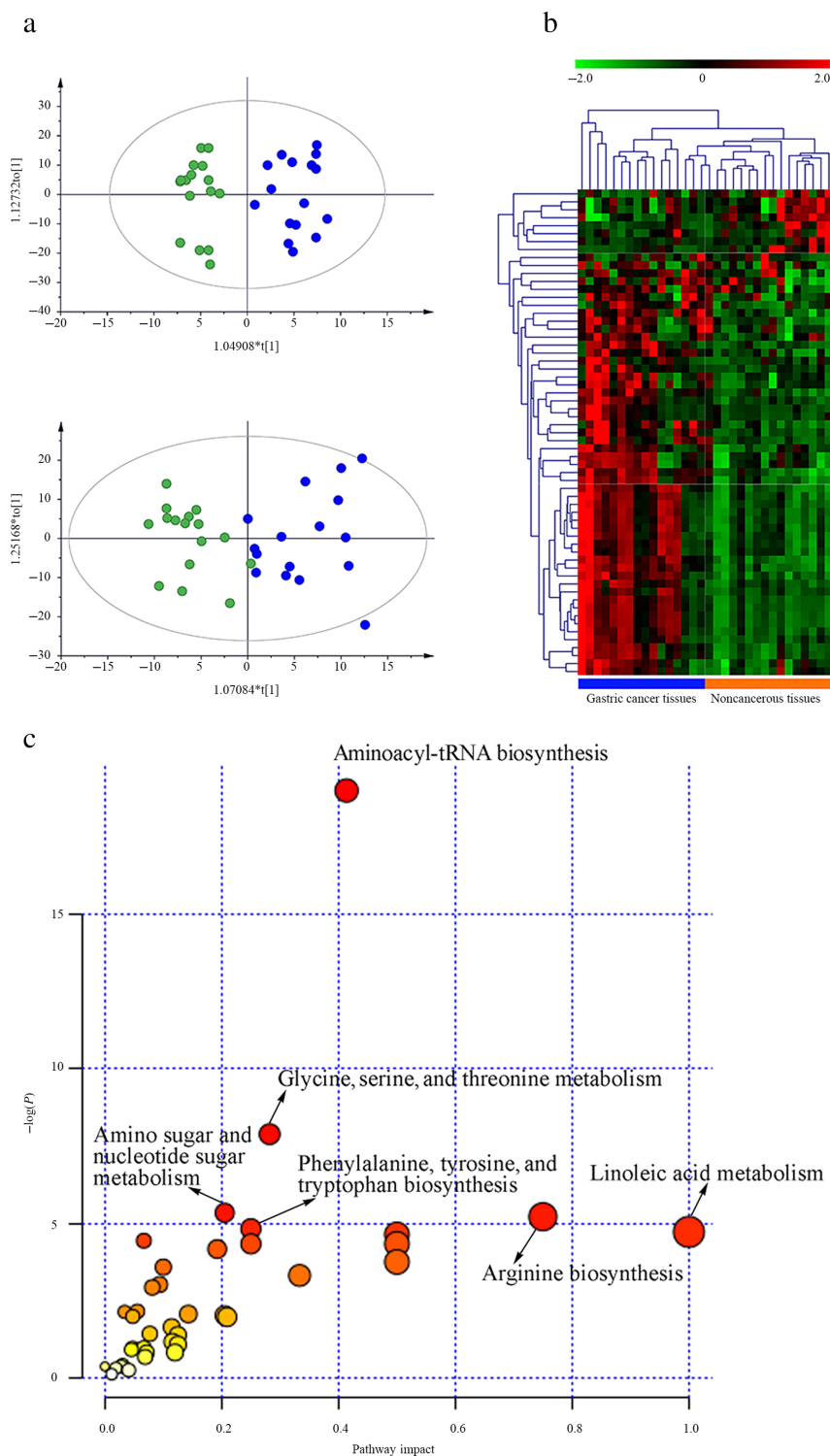
Figure 1 Distribution of differential metabolites and metabolic pathways in gastric cancer. (a) The score plot of the orthogonal partial least squares discriminant analysis model for the gastric cancer and adjacent noncancerous tissues based on liquid chromatography–tandem mass spectrometry data. Green dots represent cancer tissues, while blue dots represent adjacent noncancerous tissues. (b) Heatmap visualization of the metabolomics data of the gastric cancer and adjacent noncancerous tissues. The horizontal axis indicates the samples, while the vertical axis indicates the metabolites. (c) Distribution of metabolite-matched metabolism pathways based on the scores from topology analysis (*x*-axis) and enrichment analysis (*y*-axis). Each circle represents the matched metabolism pathways. The circle color and size were based on pathway *P* value and impact value, respectively.

metabolism; amino sugar and nucleotide sugar metabolism; phenylalanine, tyrosine, and tryptophan biosynthesis; and arginine biosynthesis were the top 5 dysregulated metabolic pathways in GC tissues.

Aminoacyl-tRNA biosynthesis pathway is upregulated in the metabolome and transcriptome. Metabolic pathways are regulated mainly by metabolizing enzymes. The mRNA expression levels of metabolizing enzymes in the

Table 1 Key differential metabolites in positive electrospray ionization (ESI+) mode of liquid chromatography–tandem mass spectrometry

No.	Metabolite	HDMB ID	KEGG ID	*m/z*	RT	VIP	FC	*P* value	Metabolic pathway
1	D-Proline	HMDB0003411	C00763	116.07	291.40	14.64	1.25	8.17E − 04	Amino acids
2	Uracil	HMDB0000300	C00106	113.03	70.25	5.56	2.02	1.28E − 03	Pyrimidines
3	1,2-Dioleoyl-*sn*-glycero-3-phosphocholine	HMDB0062690	NA	832.59	126.02	2.67	1.57	1.83E − 03	Phosphatidylcholines
4	L-Glutamate	HMDB0000148	C00025	148.06	370.62	6.43	1.33	3.37E − 03	Amino acids
5	L-Norleucine	HMDB0001645	C01933	263.20	242.98	1.81	1.56	3.46E − 03	Amino acids
6	Dopamine	HMDB0000073	C03758	136.08	280.37	4.61	1.34	4.11E − 03	Catecholamines
7	1-Aminocyclopropanecarboxylic acid	HMDB0036458	NA	84.04	370.62	3.74	1.28	4.97E − 03	Amino acids
8	γ-L-Glutamyl-L-phenylalanine	HMDB0000594	NA	295.13	319.22	1.05	1.73	5.36E − 03	Amino acids
9	*trans*-3-Coumaric acid	HMDB0001713	C12621	147.04	280.38	1.81	1.29	5.73E − 03	Hydroxycinnamic acids
10	*trans*-2-Hydroxycinnamic acid	HMDB0002641	C01772	165.06	280.36	4.83	1.32	6.66E − 03	Hydroxycinnamic acids
11	Acetylcarnitine	HMDB0000201	C02571	204.12	286.13	26.23	0.78	6.95E − 03	Acyl carnitines
12	L-Phenylalanine	HMDB0000159	C00079	166.09	236.11	11.12	1.31	7.12E − 03	Amino acids
13	L-Tyrosine	HMDB0000158	C00082	182.08	280.32	6.15	1.32	7.50E − 03	Amino acids
14	Tyramine	HMDB0000306	C00483	120.08	235.86	15.28	1.31	7.86E − 03	Phenethylamines
15	L-Leucine	HMDB0000687	C00123	132.10	242.69	8.29	1.27	7.99E − 03	Amino acids
16	Betaine	HMDB0000043	C00719	118.09	279.46	4.21	1.28	9.38E − 03	Amino acids
17	Phenyllactic acid	HMDB0000779	C01479	149.06	236.21	1.94	1.31	1.09E − 02	Phenylpropanoic acids
18	L-Proline	HMDB0000162	C00148	231.13	291.91	2.06	1.28	1.16E − 02	Amino acids
19	D-Mannose	HMDB0000169	C00159	145.05	285.65	3.25	0.79	1.19E − 02	Carbohydrates
20	5-Hydroxyindoleacetate	HMDB0000763	C05635	192.07	241.71	2.05	2.41	1.26E − 02	Indoles
21	*N*-Acetylneuraminic acid	HMDB0000230	C19910	310.11	349.21	1.31	1.57	1.30E − 02	Carbohydrates
22	3-(3-Hydroxyphenyl)propanoic acid	HMDB0000375	C11457	131.05	236.23	1.58	1.26	1.33E − 02	Phenylpropanoic acids
23	Indole	HMDB0000738	C00463	118.06	237.73	1.72	1.32	1.38E − 02	Indoles
24	L-Phenylalanine	HMDB0000159	C00079	331.17	235.60	1.63	1.46	1.68E − 02	Amino acids
25	L-Kynurenine	HMDB0000684	C00328	209.09	241.57	2.48	2.36	1.72E − 02	Carbonyl compounds
26	L-Aspartate	HMDB0000191	C00049	134.04	376.26	2.29	1.41	1.90E − 02	Amino acids
27	Mannose-6-phosphate	HMDB0001078	C00275	225.02	448.84	1.66	1.36	1.91E − 02	Carbohydrates
28	L-Tryptophan	HMDB0000929	C00078	205.10	238.42	5.49	1.32	2.19E − 02	Indoles
29	1,2-Dioleoyl-*sn*-glycero-3-phosphocholine	HMDB0062690	NA	808.59	127.01	6.93	1.41	2.37E − 02	Glycerophospholipids
30	Indole-3-lactic acid	HMDB0000958	C02341	188.07	238.33	7.22	1.28	2.38E − 02	NA
31	Valylisoleucine	HMDB0029130	NA	231.17	179.54	1.02	1.89	2.46E − 02	Amino acids
32	N^2,N^2-Dimethylguanosine	HMDB0004824	NA	312.13	178.09	1.56	1.65	2.64E − 02	Purine nucleosides
33	PC(16:0/16:0)	HMDB0000564	C00157	756.56	45.54	2.28	1.32	2.79E − 02	Glycerophospholipids
34	L-Pyroglutamic acid	HMDB0000267	C01879	147.08	351.94	3.60	1.36	2.89E − 02	Amino acids
35	D-Alanyl-D-alanine	HMDB0003459	C00993	161.09	74.74	1.11	2.37	3.08E − 02	Amino acids
36	D-Glucose 6-phosphate	HMDB0001401	C00668	261.04	448.85	2.35	1.33	3.75E − 02	Carbohydrates
37	*N*-Acetylmannosamine	HMDB0001129	C00645	222.10	240.50	4.31	1.51	3.84E − 02	Carbohydrates
38	4-Imidazoleacetic acid	HMDB0002024	C02835	127.05	298.63	2.05	1.74	4.46E − 02	Imidazoles

FC, fold change; HMDB, Human Metabolome Database; KEGG, Kyoto Encyclopedia of Genes and Genomes; RT, retention time; VIP, variable importance in the projection.

GC tissues were downloaded from TCGA database and ranked using the GSEA software. The metabolic pathways potentially involved in GC were analyzed by clustering the metabolizing enzyme sets. The analysis revealed that 24 pathways were significantly altered between GC tissues and adjacent noncancerous tissues ($P < 0.05$) and these pathways were ranked using the normalized ES score. The aminoacyl-tRNA biosynthesis pathway was one of the top 10 pathways (Fig. 2). The genes enriched in this pathway were upregulated (Table S5).

Metabolome and transcriptome analyses revealed that 15 and 24 metabolic pathways were significantly dysregulated in GC, respectively. Hence, a crossed pathway analysis was performed. The aminoacyl-tRNA pathway was identified as the aberrant pathway in the metabolome and transcriptome of the GC tissues (Fig. 3a).

The aminoacyl-tRNA biosynthesis pathway was composed of 13 interactive metabolites that were upregulated in GC (Fig. 3b). Additionally, the mRNA levels of 31 metabolism-related genes in the aminoacyl-tRNA biosynthesis pathway were upregulated in GC (Table S4 and Fig. 3c). These findings suggest that the aminoacyl-tRNA biosynthesis pathway is significantly upregulated in GC.

To visualize the interaction between the metabolites and their potential metabolizing enzymes in aminoacyl-tRNA biosynthesis, a metabolite–enzyme interaction network was constructed (Fig. 4). The interaction network consisted of 12 aminoacyl-tRNA synthetases (ARSs) and 13 metabolites. To synthesize the corresponding aminoacyl-tRNA, 12 upregulated core enzymes interact with 13 metabolites. These results indicate that

Table 2 Key differential metabolites in negative electrospray ionization (ESI−) mode of liquid chromatography–tandem mass spectrometry

No.	Metabolite	HDMB ID	KEGG ID	*m/z*	RT	VIP	FC	*P* value	Metabolic pathway
1	Glycine	HMDB0000123	C00037	74.02	343.00	1.93	1.35	6.75E − 04	Amino acids
2	D-Tagatose	HMDB0003418	C00795	201.04	373.81	1.23	0.69	7.75E − 04	Carbohydrates
3	*N*-Acetylmannosamine	HMDB0001129	C00645	220.08	239.88	3.12	1.92	2.86E − 03	Carbohydrates
4	L-Serine	HMDB0003406	C00740	104.03	355.80	2.09	1.28	4.44E − 03	Amino acids
5	D-Proline	HMDB0003411	C00763	114.06	290.37	5.95	1.38	4.49E − 03	Amino acids
6	L-Threonine	HMDB0000167	C00188	118.05	332.69	2.91	1.37	4.65E − 03	Amino acids
7	Uracil	HMDB0000300	C00106	111.02	69.80	11.74	1.62	6.96E − 03	Pyrimidines
8	L-Asparagine	HMDB0000168	C00152	131.04	356.41	1.52	1.31	7.27E − 03	Amino acids
9	L-Threonic acid	HMDB0062620	NA	135.03	310.76	1.75	1.37	8.25E − 03	Carbohydrates
10	*N*-Acetyl-L-alanine	HMDB0000766	NA	130.05	226.92	2.19	1.47	9.27E − 03	Amino acids
11	L-Glutamate	HMDB0000148	C00025	146.05	369.68	5.86	1.25	9.42E − 03	Amino acids
12	Sarcosine	HMDB0000271	C00213	88.04	226.96	1.57	1.40	9.62E − 03	Amino acids
13	L-Kynurenine	HMDB0000684	C00328	207.07	241.09	1.13	3.00	1.07E − 02	Organooxygen compound
14	Ribothymidine	HMDB0000884	NA	257.07	56.32	1.11	1.84	1.12E − 02	Pyrimidine nucleosides
15	L-Phenylalanine	HMDB0000159	C00079	164.07	236.55	11.71	1.43	1.15E − 02	Amino acids
16	2E-Eicosenoic acid	NA	NA	309.28	40.52	7.10	0.61	1.26E − 02	NA
17	L-Aspartate	HMDB0000191	C00049	132.03	375.05	3.59	1.46	1.26E − 02	Amino acids
18	Indolelactic acid	HMDB0000671	C02043	204.07	34.64	2.31	1.92	1.29E − 02	Indoles
19	1-Deoxy-D-xylulose 5-phosphate	HMDB0001213	C11437	273.04	380.15	1.25	0.48	1.29E − 02	Carbohydrates
20	L-Tyrosine	HMDB0000158	C00082	180.07	279.91	6.93	1.32	1.35E − 02	Amino acids
21	*N*-Acetylneuraminic acid	HMDB0000230	C19910	308.10	348.74	1.44	1.60	1.44E − 02	Carbohydrates
22	4-Hydroxycinnamic acid	HMDB0002035	C00811	163.04	279.89	1.39	1.30	1.56E − 02	Hydroxycinnamic acids
23	Linoleic acid	HMDB0000673	C01595	301.21	41.00	6.86	1.44	1.62E − 02	Fatty acyls
24	α-D-Glucose 1-phosphate	HMDB0001586	C00103	241.01	372.66	1.15	0.52	1.79E − 02	Carbohydrates
25	Pentadecanoic acid	HMDB0000826	C16537	241.21	43.33	1.84	1.28	2.04E − 02	Fatty acyls
26	L-Tryptophan	HMDB0000929	C00078	203.08	237.93	4.86	1.31	2.45E − 02	Indoles
27	Thymine	HMDB0000262	C00178	125.03	47.11	1.02	1.87	2.96E − 02	Pyrimidines
28	L-Methionine	HMDB0000696	C00073	148.04	262.47	3.67	1.42	3.01E − 02	Amino acids
29	Glycerol 3-phosphate	HMDB0000126	C00093	171.00	411.25	1.13	0.44	3.06E − 02	Glycerophospholipids
30	Adipic acid	HMDB0000448	C06104	145.05	316.00	1.39	0.38	3.12E − 02	Fatty acyls
31	Glyoxylate	HMDB0000119	C00048	72.99	57.40	2.18	1.56	4.09E − 02	Carboxylic acids
32	L-lactate	HMDB0000190	C00186	80.92	280.79	1.13	2.28	8.00E − 02	Amino acids
33	L-Glutamine	HMDB0000641	C00064	145.06	351.58	3.35	1.22	9.58E − 02	Amino acids

FC, fold change; HMDB, Human Metabolome Database; KEGG, Kyoto Encyclopedia of Genes and Genomes; RT, retention time; VIP, variable importance in the projection.

the aminoacyl-tRNA biosynthesis pathway is upregulated in GC owing to the overexpression of 12 ARSs.

Characteristics of metabolic enzymes of the aminoacyl-tRNA biosynthesis pathway in gastric cancer.

The role of 12 key synthetases of the aminoacyl-tRNA biosynthesis pathway in GC was examined. The correlation between the mRNA expression levels of 12 key ARSs and clinical characteristics in patients with GC was investigated based on TCGA database. Among the key ARSs, the upregulated expression of FARSB was associated with poor overall survival (OS) rate and clinical outcomes in patients with GC (Fig. 5a). The Wilcoxon test indicated that the expression level of TARS in G2 and G3 grade tumors was significantly higher than that in G1 grade tumors (Fig. 5b). However, the expression of other ARSs did not significantly vary according to the GC grade, TNM stage, and survival status. Further studies are needed to examine the role of ARSs in GC development. These data suggest that FARSB is a potential prognostic factor for OS and that the upregulated expression of TARS is correlated with the pathological grade of GC.

Overexpression of threonyl-tRNA synthetase and phenylalanyl-tRNA synthetase is correlated with the development of gastric cancer.

The protein expression and subcellular location of TARS and FARSB were determined using TMA consisting of 98 GC tissues and 82 adjacent noncancerous gastric mucosal tissues. As shown in Figure 6a–d, TARS and FARSB were mainly localized in the cytoplasm of gastric basal cells and cancer cells. The expression levels of TARS and FARSB were upregulated in 64.3% (63/98) and 74.5% (73/98) of GC tissues, respectively. In contrast, the expression levels of TARS and FARSB were upregulated in only 35.4% (29/82) and 26.8% (22/82) of the noncancerous tissues, respectively. Furthermore, the IHC scores of TARS and FARSB in the GC tissues were significantly higher than those in the adjacent noncancerous tissues (Fig. 6e). These data indicate that TARS and FARSB are overexpressed in GC tissues.
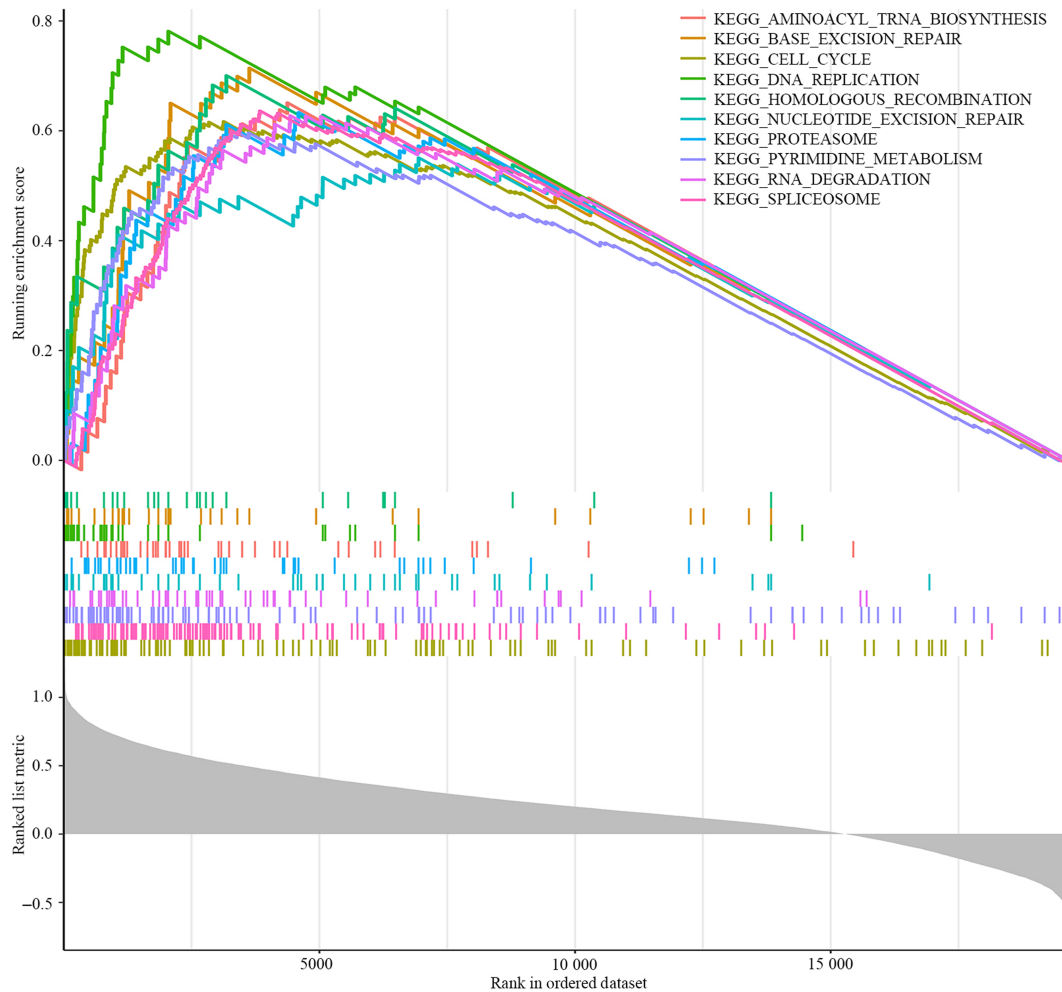
Figure 2 Top 10 significantly enriched pathways in the transcriptomic data from The Cancer Genome Atlas Stomach Adenocarcinoma dataset. KEGG, Kyoto Encyclopedia of Genes and Genomes. —, KEGG_AMINOACYL_TRNA_BIOSYNTHESIS; —, KEGG_BASE_EXCISION_REPAIR; —, KEGG_CELL_CYCLE; —, KEGG_DNA_REPLICATION; —, KEGG_HOMOLOGOUS_RECOMBINATION; —, KEGG_NUCLEOTIDE_EXCISION_REPAIR; —, KEGG_PROTEASOME; —, KEGG_PYRIMIDINE_METABOLISM; —, KEGG_RNA_DEGRADATION; —, KEGG_SPLICEOSOME.

The GC samples were divided into TARS/FARSB-high and TARS/FARSB-low groups according to the median IHC score. Consistent with the findings in TCGA cohort, the OS of the FARSB-high group was poorer than that of the FARSB-low group (Fig. 6h). Furthermore, FARSB overexpression was significantly correlated with the progression of the M stage (Fig. 6f) rather than that of the pathology grades, T and N stages. TARS expression was significantly associated with poor survival (Fig. 6g). These results confirmed that upregulated FARSB expression levels in GC tissues were correlated with tumor metastasis and prognosis. The correlation between TARS/FARSB and five prognostic markers (VEGFR, P53, CD133, Ki67, and E-cadherin) was also assessed to validate the role of TARS and FARSB in GC (Fig. 7). The expression levels of TARS and FARSB were significantly correlated with those of VEGFR, which indicated that the upregulated expression of TARS/FARSB was associated with tumor metastasis. Additionally, the expression of FARSB was significantly correlated with

that of P53 and CD133. This finding suggested that the upregulated expression of FARSB was associated with tumor proliferation. The expression levels of TARS/FARSB were not correlated with those of Ki67 and E-cadherin. These results indicate that TARS and FARSB are associated with tumor metastasis and proliferation in GC.

Thus, the upregulated expression of TARS and FARSB, which are metabolic enzymes in the aminoacyl-tRNA biosynthesis pathway, is associated with gastric tumor metastasis and proliferation and poor prognosis.

Discussion

Gastric cancer is the fifth most common cancer and the second leading cause of cancer-related mortality.[13] Several risk factors, including *Helicobacter pylori* infection, environmental factors, and genetic susceptibility, have been reported for GC. However, the pathogenetic mechanism of GC has not been elucidated.[14,15]
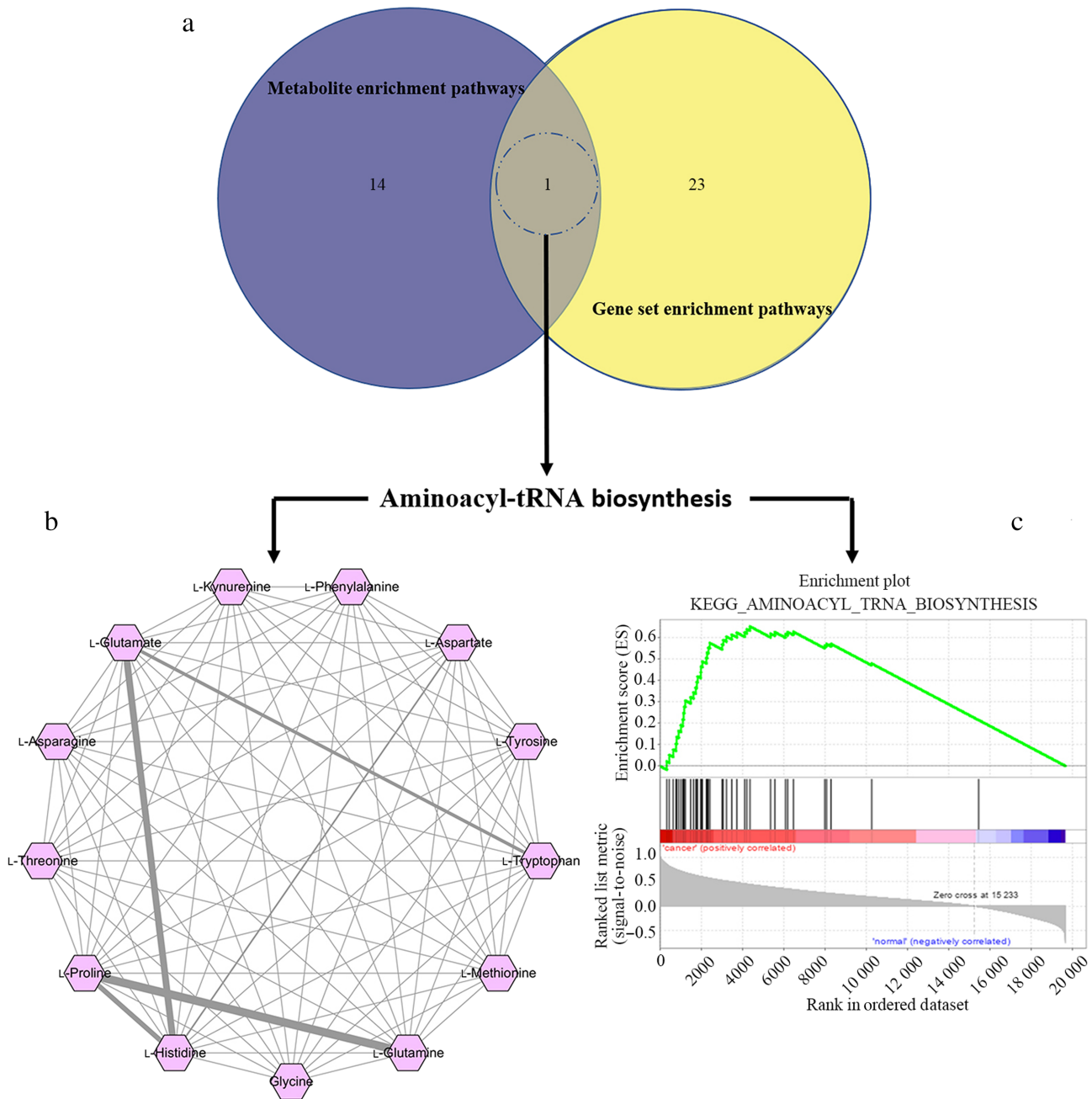
Figure 3 Integrated analysis of metabolites and genes enriched in different pathways. (a) Venn diagram of the pathways in which differential metabolites and genes are enriched. (b) Interaction of differential metabolites in the aminoacyl-tRNA biosynthesis pathway. (c) Enrichment plots of genes clustered in the aminoacyl-RNA biosynthesis pathway using Gene Set Enrichment Analysis. The blank line in the middle represents the altered gene. The green line represents normalized enrichment score (ES). ▬, enrichment profile; ▬, hits; ▬, ranking metric scores.

Currently, surgery and chemoradiotherapy are the major therapeutic strategies for GC. However, the efficacy of these therapeutic strategies has plateaued.[16,17] Therefore, there is a need to identify novel biomarkers for disease progression and therapeutic outcomes. In this study, metabolomic and transcriptomic data were integrated to identify the key metabolic pathways in GC. The findings of this study indicated that the aminoacyl-tRNA pathway was upregulated in both the metabolome and transcriptome of GC. Furthermore, TARS and FARSB, which are two metabolic enzymes of the aminoacyl-tRNA biosynthesis pathway, were involved in the progression of GC. This study provides useful insights for developing novel therapeutic strategies for GC by targeting the aminoacyl-tRNA biosynthesis pathway and its key metabolic enzymes.
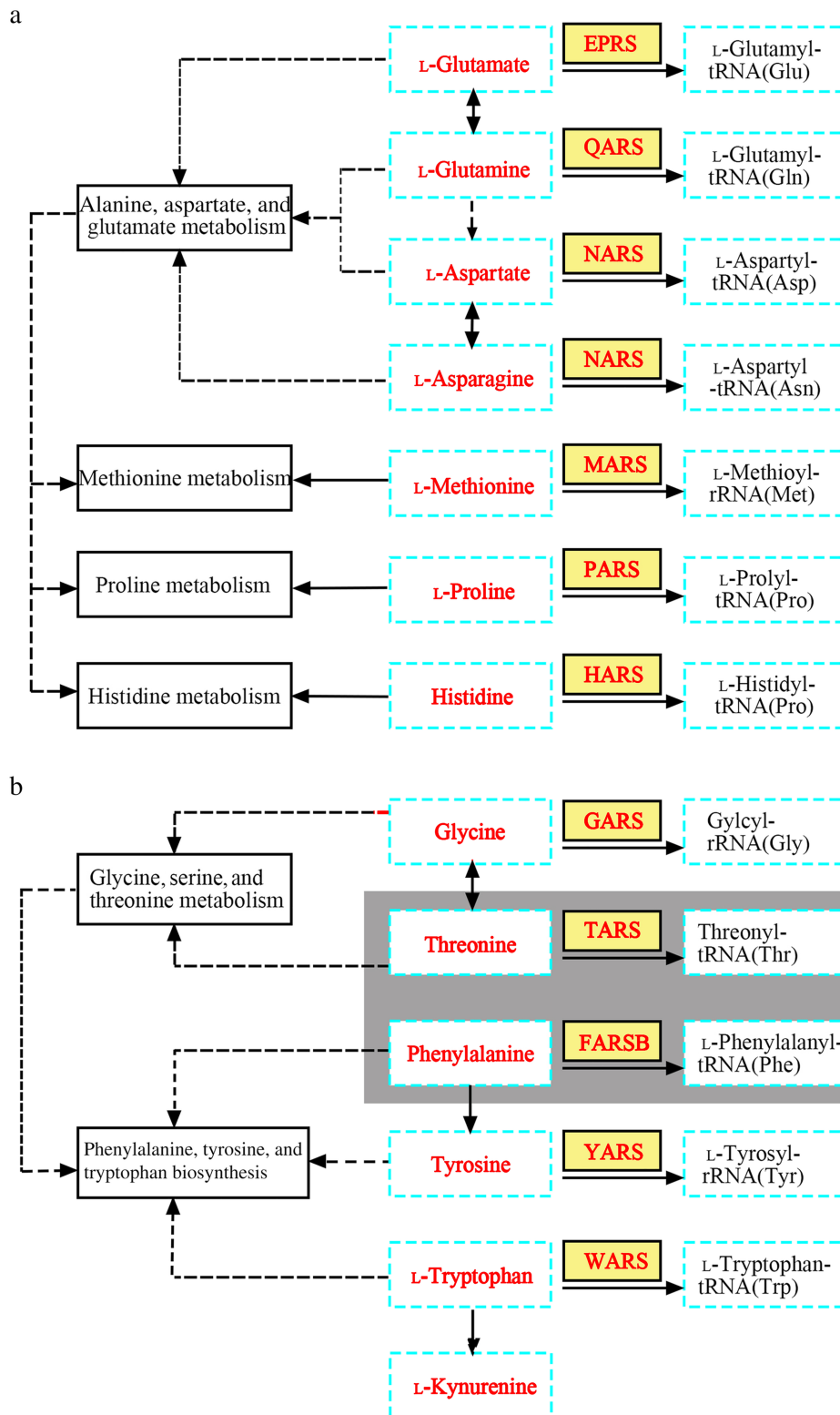
Figure 4   Interaction network of differential metabolites and genes in the aminoacyl-tRNA biosynthesis pathway. Red colored nodes represent upregulated metabolites and aminoacyl-tRNA synthetases in gastric cancer. Blue and yellow rectangles indicate metabolite in the aminoacyl-tRNA biosynthesis pathway and aminoacyl-tRNA synthetases, respectively. (a) Aminoacyl-tRNA synthetases and metabolites involved in alanine, aspartate, and glutamate metabolism and its related downstream metabolic pathways. (b) Aminoacyl-tRNA synthetases and metabolites involved in glycine, serine, and threonine metabolism and its related downstream metabolic pathways.
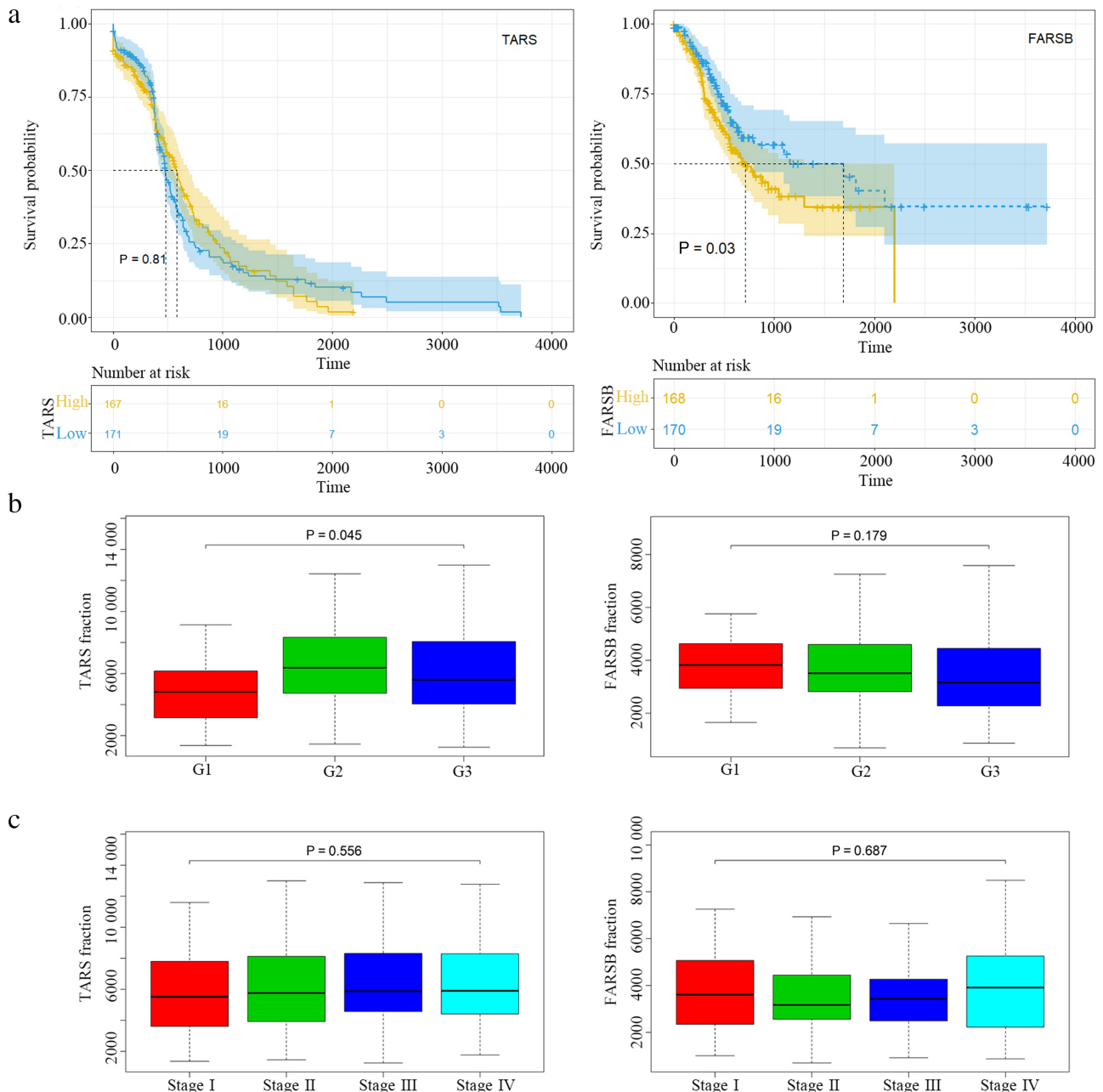
Figure 5 Stratification analysis based on the expression levels of threonyl-tRNA synthetase (TARS) and phenylalanyl-tRNA synthetase (FARSB) and clinical outcome in gastric cancer (GC). (a) The overall survival analysis result is indicated in the left column. TARS: ▢, high; ▢, low. FARSB: ▢, high; ▢, low. (b) The prognostic significance of TARS was evaluated based on GC grade status. (c) The prognostic significance of FARSB was evaluated based on GC stage status.

Metabolic pathways are reprogrammed to maintain cancer cell proliferation and survival. The reprogramming of metabolic pathways involves the metabolism of glucose, amino acids, and lipids. Most cancer cells metabolize glucose through glycolysis to meet the high demand for adenosine triphosphate instead of oxidative phosphorylation through the tricarboxylic acid cycle.[18] The less efficient adenosine triphosphate generation through glycolysis is rationalized by providing available glycolytic intermediates for the biosynthesis of amino acids, lipids, and nucleosides. The

Warburg effect can also enhance lactate generation in GC.[19] In this study, the levels of carbohydrates were low, whereas those of lactate were high in the GC tissues, which confirmed the Warburg effect in GC. The alterations in the expression of genes encoding key catalytic enzymes or regulators in metabolic pathways must also be identified. For example, indoleamine 2,3-dioxygenase (IDO) is the rate-limiting enzyme for the production of kynurenine.[20] Therefore, the LC–MS/MS-based metabolome data were integrated with the transcriptome data from TCGA database to
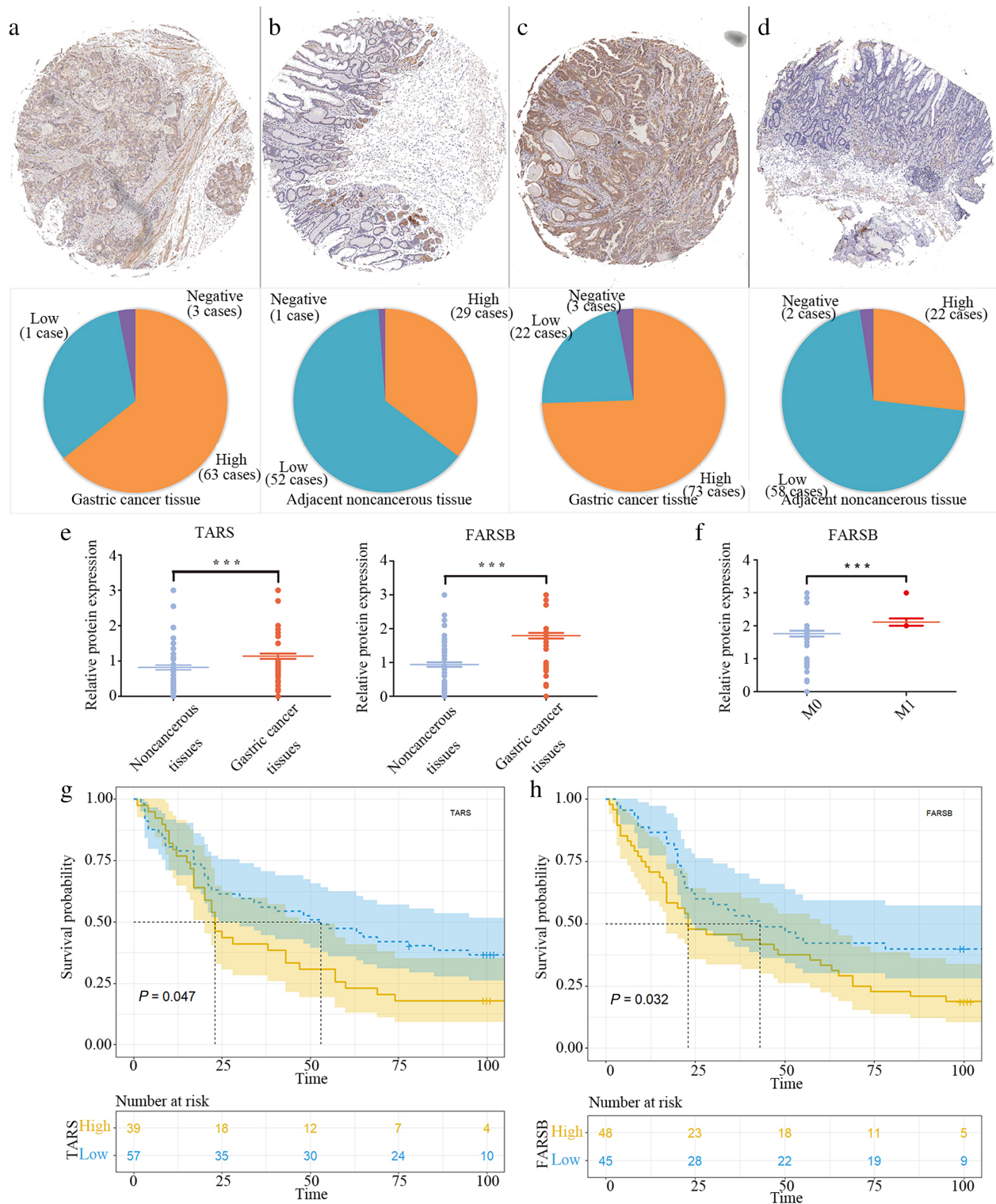
Figure 6 Correlation of the expression levels of threonyl-tRNA synthetase (TARS) and phenylalanyl-tRNA synthetase (FARSB) in gastric cancer (GC) and its pathological significance. (a, b) Representative immunohistochemical staining of TARS in cancer and noncancerous tissues. (c, d) Representative immunohistochemical staining of FARSB in cancer and adjacent noncancerous tissues. (e) Protein expression levels of TARS and FARSB in the tissue microarray samples. (f) The expression level of FARSB is correlated with distant metastasis of GC. (g) Kaplan–Meier survival curve of patients with GC in the TARS-low and TARS-high groups. TARS: ▬, high; ▬, low. (h) Kaplan–Meier survival curve of patients with GC in the FARSB-low and FARSB-high groups. FARSB: ▬, high; ▬, low.
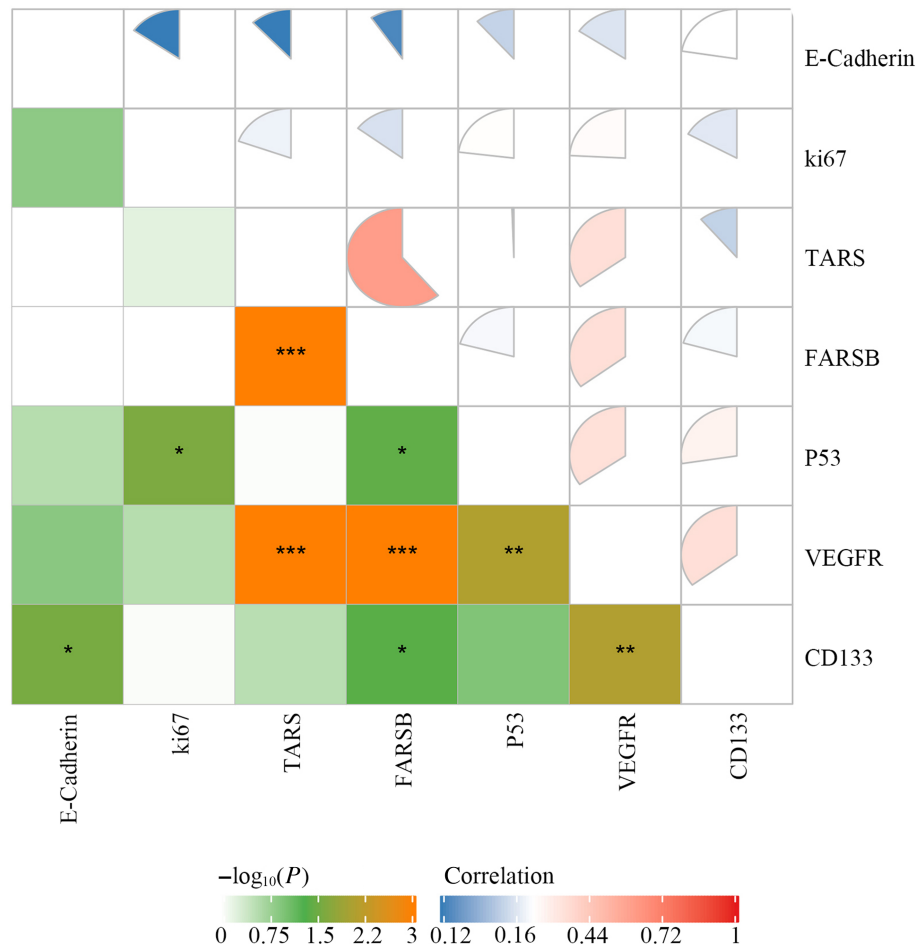
Figure 7 Correlation between threonyl-tRNA synthetase (TARS), phenylalanyl-tRNA synthetase (FARSB), and gastric cancer-related prognostic immunohistochemical markers. The circle size and color on the upper right of image indicate the correlation coefficient value. The colored square on the bottom left of the image represents the value of $-\log_{10}(P)$. *$P < 0.001$, **$P < 0.01$, and ***$P < 0.05$.

examine the metabolomic changes in GC. A gene–metabolite interaction network consisting of both metabolic enzymes and metabolites was constructed to model the specific metabolic pathways.

The integrated analysis revealed the upregulation of the aminoacyl-tRNA biosynthesis pathway in GC. To the best of our knowledge, this is the first study to highlight the role of the aminoacyl-tRNA biosynthesis pathway in GC based on the integration of both metabolomic and transcriptomic data. The findings of this study are consistent with those of a previous study, which demonstrated that the aminoacyl-tRNA biosynthesis pathway is markedly upregulated in the GC cell lines using single metabonomics.[21] ARSs are the major regulators of the aminoacyl-tRNA biosynthesis pathway.[22] Hence, the mRNA expression levels of metabolic enzymes in GC tissues were analyzed. The aminoacyl-tRNA biosynthesis pathway was upregulated at the transcript level. This finding can contribute to the elucidation of the complex mechanisms of metabolic disorders associated with cancer.

Previous studies have reported that metabolites, which are important substrates of peptide bonds and protein synthesis, are potential prognostic and diagnostic biomarkers for specific tumor development.[23,24] Among the 71 differentially expressed metabolites, 13 were upregulated in the aminoacyl-tRNA biosynthesis pathway in GC. Consistent with previous studies on urine metabolomics in GC, this study reported that proline was significantly upregulated in GC tissues. Compared with its role in nonmetastatic GC, proline has a critical role in metastatic GC.[25] Treatment with proline degradation enzyme inhibitors downregulated cancer cell metastasis.[26] Tryptophan and kynurenine are reported to be dysregulated in GC. The dysregulation of the tryptophan/kynurenine catabolism pathway is associated with poor prognosis in GC.[27] In this study, the levels of tryptophan and kynurenine were upregulated in GC tissues. However, the ratio of tryptophan/kynurenine markedly decreased in GC tissues. This is because IDO catalyzes tryptophan catabolism, which leads to the production of toxic kynurenine. IDO has been proposed to function as an immune suppressor and induce immune tolerance. Various studies have reported that the expression of IDO is upregulated in the tumor microenvironment and that the upregulated IDO expression is correlated with immune suppression and cancer progression.[28,29] Kynurenine, which is the main metabolite of IDO-catalyzed

tryptophan catabolism, was the most upregulated metabolite in this study. Therefore, further studies are needed to determine the potential role of proline, kynurenine, and IDO in GC diagnosis and therapy.

Bioinformatic analysis of TCGA database and verification experiments using TMA were performed. This study, for the first time, demonstrated that among the ARSs of the aminoacyl-tRNA biosynthesis pathway, the upregulated expression levels of TARS and FARSB were correlated with tumor metastasis and proliferation in GC. In addition to their functions in protein synthesis, ARSs are involved in various cellular processes, such as immune and inflammatory responses, angiogenesis, and apoptosis.[30,31] Additionally, recent studies have reported that ARSs are involved in the oncogenesis pathways by binding to ARS-interacting proteins. For example, methionyl-tRNA synthetase binds to CDK4 to promoteo cell cycle,[32] while glutaminyl-tRNA synthetase binds to ASK1 to regulate cell apoptosis.[33] Several ARSs function as secreted cytokines to shape the tumor microenvironment. The secreted tyrosyl-tRNA synthetase harbors a specific ELR (Glu–Leu–Arg) motif in its N-terminal domains, which promotes polymorphonuclear cell migration and stimulates angiogenesis.[34] Hence, future studies must focus on ARSs to gain novel insights into the pathogenic process and develop potential therapeutic strategies for GC. However, the precise role of other ARSs (e.g. DARS, PARS, and EPRS) involved in the catalytic steps of aminoacyl-tRNA biosynthesis is an active area of research.

This study demonstrated that the upregulated expression of TARS was positively correlated with poor prognosis in GC. TARS is an angiogenesis-regulating factor as it stimulates the migration of vascular endothelial cells and promotes the formation of blood vessel.[35] Previous studies reported that TARS overexpression was positively correlated with the stage of ovarian cancer[36] and pancreatic cancer cell migration.[37] Our data confirmed elevated TARS expression in GC tissues and paralleled to expression level of VEGFR, an important angiogenic signaling molecule. Although the correlation between TARS expression and GC stage was not significant, the expression of TARS was upregulated in advanced stages of GC. Therefore, TARS may be a novel anti-metastatic therapeutic target for GC. Further studies are needed to elucidate the molecular mechanisms of TARS in GC and determine its potential as a therapeutic target for GC.

The analysis of Human Protein Atlas revealed that FARSB is a potential prognostic indicator for some cancers.[38,39] Currently, most studies focus on the correlation between FARSB mutations and interstitial lung disease, hypotonia, liver cirrhosis, and so forth.[40] However, limited studies have focused on the role of FARSB in GC development. This study demonstrated that the expression of FARSB is upregulated in GC tissues. Additionally, the upregulated expression of FARSB was correlated with distant metastasis and poor survival in GC. Mechanistically, FARSB is the target protein of IGFBP7,[41] which regulates anti-apoptotic signaling and cell proliferation[42] by interacting with IGF-1R. However, the ability of FARSB to regulate the IGFBP7/IGF-1R axis and consequently promote oncogenesis and development in GC requires further exploration.

In conclusion, this study revealed that the aminoacyl-tRNA biosynthesis pathway is upregulated in GC based on the integrated analysis of metabolome and transcriptome of GC. The upregulated expression of TARS and FARSB, which are the key enzymes in the aminoacyl-tRNA biosynthesis pathway, was correlated with tumor metastasis and proliferation in GC. Therefore, the findings of this study will provide a basis to develop novel therapeutic strategies and diagnostic biomarkers for GC by targeting the aminoacyl-tRNA biosynthesis pathway and its key metabolic enzymes, such as TARS and FARSB.

Acknowledgment

Data availability statement

The metabolomics datasets and the clinical metadata generated in this study were submitted to MetaboLights (https://www.ebi.ac.uk/metabolights/), under accession number MTBLS1814.

References

1 Zhuang H, Li Q, Zhang X *et al*. Downregulation of glycine decarboxylase enhanced cofilin-mediated migration in hepatocellular carcinoma cells. *Free Radic. Biol. Med.* 2018; **120**: 1–12.

2 Kwon HN, Lee H, Park JW, Kim Y-H, Park S, Kim JJ. Screening for early gastric cancer using a noninvasive urine metabolomics approach. *Cancer* 2020; **12**: 2904.

3 Liu Y, Zhang Z, Wang J *et al*. Metabolic reprogramming results in abnormal glycolysis in gastric cancer: a review. *Onco. Targets. Ther.* 2019; **12**: 1195–204.

4 Lee J-Y, Nam M, Son HY *et al*. Polyunsaturated fatty acid biosynthesis pathway determines ferroptosis sensitivity in gastric cancer. *Proc. Natl. Acad. Sci. U. S. A.* 2020; **117**: 32433–42.

5 Charitou T, Srihari S, Lynn MA *et al*. Transcriptional and metabolic rewiring of colorectal cancer cells expressing the oncogenic KRAS^{G13D} mutation. *Br. J. Cancer* 2019; **121**: 37–50.

6 Schaeffeler E, Büttner F, Reustle A *et al*. Metabolic and lipidomic reprogramming in renal cell carcinoma subtypes reflects regions of tumor origin. *Eur. Urol. Focus* 2019; **5**: 608–18.

7 Maldonado LY, Arsene D, Mato JM, Lu SC. Methionine adenosyltransferases in cancers: mechanisms of dysregulation and implications for therapy. *Exp. Biol. Med. (Maywood)* 2018; **243**: 107–17.

8 Mishra P, Tang W, Putluri V *et al*. ADHFE1 is a breast cancer oncogene and induces metabolic reprogramming. *J. Clin. Invest.* 2018; **128**: 323–40.

9 Gao B, Lue H-W, Podolak J *et al*. Multi-omics analyses detail metabolic reprogramming in lipids, carnitines, and use of glycolytic intermediates between prostate small cell neuroendocrine carcinoma and prostate adenocarcinoma. *Metabolites* 2019; **9**: 82.

10 Domingo-Almenara X, Montenegro-Burke J, Ivanisevic J *et al*. XCMS-MRM and METLIN-MRM: a cloud library and public resource for targeted analysis of small molecules. *Nat. Methods* 2018; **15**: 681–4.

11 Wang S, Chen X, Dan D *et al*. MetaboGroup S: a group entropy-based web platform for evaluating normalization methods in blood metabolomics data from maintenance hemodialysis patients. *Anal. Chem.* 2018; **90**: 11124–30.

12 Xia J, Psychogios N, Young N, Wishart D. MetaboAnalyst: a web server for metabolomic data analysis and interpretation. *Nucleic Acids Res.* 2009; **37**: W652–60.

13 Mizrak Kaya D, Harada K, Shimodaira Y, Amlashi F, Lin Q, Ajani J. Advanced gastric adenocarcinoma: optimizing therapy options. *Expert Rev. Clin. Pharmacol.* 2017; **10**: 263–71.

14 Miernyk KM, Bulkow LR, Gold BD *et al*. Prevalence of *Helicobacter pylori* among Alaskans: factors associated with infection and comparison of urea breath test and anti-*Helicobacter pylori* IgG antibodies. *Helicobacter* 2018; **23**: e12482.

15 Russo AE, Strong VE. Gastric cancer etiology and management in Asia and the West. *Annu. Rev. Med.* 2019; **70**: 353–67.

16 Wu A, Ji J. Adjuvant chemotherapy for gastric cancer or not: a dilemma? *J. Natl. Cancer Inst.* 2008; **100**: 376–7.

17 Brisinda G, Crocco A, Tomaiuolo P, Santullo F, Mazzari A, Vanella S. Extended or limited lymph node dissection? A gastric cancer surgical dilemma. *Ann. Surg.* 2012; **256**: e30–1.

18 Seyfried TN, Arismendi-Morillo G, Mukherjee P, Chinopoulos C. On the origin of ATP synthesis in cancer. *iScience* 2020; **23**: 101761.

19 Ping W, Senyan H, Li G, Yan C, Long L. Increased lactate in gastric cancer tumor-infiltrating lymphocytes is related to impaired T cell function due to miR-34a deregulated lactate dehydrogenase A. *Cell. Physiol. Biochem.* 2018; **49**: 828–36.

20 Puccetti P, Fallarino F, Italiano A *et al*. Accumulation of an endogenous tryptophan-derived metabolite in colorectal and breast cancers. *PLoS ONE* 2015; **10**: e0122046.

21 Li J, Wang Q, Zheng Y *et al*. Development of a mass spectrometry-based pseudotargeted metabolomics strategy to analyze hormone-stimulated gastric cancer cells. *J. Pharm. Biomed. Anal.* 2020; **180**: 113041.

22 Guo M, Schimmel P. Essential nontranslational functions of tRNA synthetases. *Nat. Chem. Biol.* 2013; **9**: 145–53.

23 Yuan B, Schafferer S, Tang Q *et al*. A plasma metabolite panel as biomarkers for early primary breast cancer detection. *Int. J. Cancer* 2019; **144**: 2833–42.

24 Sullivan LB, Gui DY, Vander HMG. Altered metabolite levels in cancer: implications for tumour biology and cancer therapy. *Nat. Rev. Cancer* 2016; **16**: 680–93.

25 Chen J, Tang H, Hu J, Fan J, Hong J, Gu J. Metabolomics of gastric cancer metastasis detected by gas chromatography and mass spectrometry. *World J. Gastroenterol.* 2010; **16**: 5874–80.

26 Phang JM. Proline metabolism in cell regulation and cancer biology: recent advances and hypotheses. *Antioxid. Redox Signal.* 2019; **30**: 635–49.

27 Patil PA, Blakely AM, Lombardo KA *et al*. Expression of PD-L1, indoleamine 2,3-dioxygenase and the immune microenvironment in gastric adenocarcinoma. *Histopathology* 2018; **73**: 124–36.

28 Amobi A, Qian F, Lugade AA, Odunsi K. Tryptophan catabolism and cancer immunotherapy targeting IDO mediated immune suppression. *Adv. Exp. Med. Biol.* 2017; **1036**: 129–44.

29 Lee H-C, Lee E-S, Uddin MB *et al*. Released tryptophanyl-tRNA synthetase stimulates innate immune responses against viral infection. *J. Virol.* 2019; **93**: e01291-18.

30 Mirando A, Francklyn C, Lounsbury K. Regulation of angiogenesis by aminoacyl-tRNA synthetases. *Int. J. Mol. Sci.* 2014; **15**: 23725–48.

31 Zhang C, Lin X, Zhao Q *et al*. YARS as an oncogenic protein that promotes gastric cancer progression through activating PI3K-Akt signaling. *J. Cancer Res. Clin. Oncol.* 2020; **146**: 329–42.

32 Kwon NH, Lee JY, Ryu Y-L *et al*. Stabilization of cyclin-dependent kinase 4 by methionyl-tRNA synthetase in p16[INK4a]-negative cancer. *ACS Pharmacol. Transl. Sci.* 2018; **1**: 21–31.

33 Ko Y-G, Kim E-K, Kim T *et al*. Glutamine-dependent antiapoptotic interaction of human glutaminyl-tRNA synthetase with apoptosis signal-regulating kinase 1. *J. Biol. Chem.* 2001; **276**: 6030–6.

34 Son S, Park M, Kim S. Extracellular activities of aminoacyl-tRNA synthetases: new mediators for cell–cell communication. *Top. Curr. Chem.* 2014; **344**: 145–66.

35 Mirando AC, Abdi K, Wo P, Lounsbury KM. Assessing the effects of threonyl-tRNA synthetase on angiogenesis-related responses. *Methods (San Diego, Calif)* 2017; **113**: 132–8.

36 Wellman TL, Eckenstein M, Wong C *et al*. Threonyl-tRNA synthetase overexpression correlates with angiogenic markers and progression of human ovarian cancer. *BMC Cancer* 2014; **14**: 620.

37 Jeong SJ, Kim JH, Lim BJ *et al*. Inhibition of MUC1 biosynthesis via threonyl-tRNA synthetase suppresses pancreatic cancer cell migration. *Exp. Mol. Med.* 2018; **50**: e424.

38 Thul PJ, Lindskog C. The Human Protein Atlas: a spatial map of the human proteome. *Protein Sci.* 2018; **27**: 233–44.

39 Dong Y-M, Li M, He Q-E *et al*. Epigenome-wide tobacco-related methylation signature identification and their multilevel regulatory network inference for lung adenocarcinoma. *Biomed. Res. Int.* 2020; **2020**: 2471915.

40 Peretz M, Tworowski D, Kartvelishvili E, Livingston J, Chrzanowska-Lightowlers Z, Safro M. Breaking a single hydrogen bond in the mitochondrial tRNA[Phe]-PheRS complex leads to phenotypic pleiotropy of human disease. *FEBS J.* 2020; **287**: 3814–26.

41 Ruan W, Wang Y, Ma Y *et al*. HSP60, a protein downregulated by IGFBP7 in colorectal carcinoma. *J. Exp. Clin. Cancer Res.: CR* 2010; **29**: 41.

42 Yoshioka T, Shien K, Namba K *et al*. Antitumor activity of pan-HER inhibitors in HER2-positive gastric cancer. *Cancer Sci.* 2018; **109**: 1166–76.

Supporting information

Additional supporting information may be found online in the Supporting Information section at the end of the article.

Table S1. Clinical information of patients in The Cancer Genome Atlas Stomach Adenocarcinoma dataset.
Table S2. Baseline characteristics of patients whose samples were used in the tissue microarray.
Table S3. Clinical information of patients whose gastric cancer samples were used for metabolomic profiling.
Table S4. Significantly altered pathways in gastric cancer.
Table S5. Genes enriched in the aminoacyl-tRNA biosynthesis pathway.
Figure S1. Representative LC-MS/MS TIC chromatograms of the sample from GC and adjacent non-cancerous tissues A and B. The TIC chromatograms of the untargeted compound in QC samples under ESI+ and ESI− conditions. C and D. The TIC chromatograms of the untargeted compound in GC tissues under ESI+ and ESI− conditions, respectively. E and F. The TIC chromatograms of the untargeted compound in NM tissues under ESI+ and ESI− conditions, respectively. LC-MS/MS, liquid chromatography-tandem mass spectrometry; TIC, total ion current; ESI+, electrospray ionisation positive mode; ESI−, electrospray ionisation negative mode; QC, quantity control; GC, gastric cancer; NM, adjacent non-cancerous tissues.